ACS APPLIED MATERIALS & INTERFACES

Research Article

www.acsami.org

Self-Enhanced Catalytic Activities of Functionalized Graphene Sheets in the Combustion of Nitromethane: Molecular Dynamic Simulations by Molecular Reactive Force Field

Chaoyang Zhang,* Yushi Wen, and Xianggui Xue

Institute of Chemical Materials, China Academy of Engineering Physics (CAEP), P.O. Box 919-327, Mianyang, Sichuan 621900, China

Supporting Information

ABSTRACT: Functionalized graphene sheet (FGS) is a promising additive that enhances fuel/propellant combustion, and the determination of its mechanism has attracted much interest. In the present study, a series of molecular dynamic simulations based on a reactive force field (ReaxFF) are performed to explore the catalytic activity (CA) of FGS in the thermal decay of nitromethane (NM, CH_3NO_2). FGSs and pristine graphene sheets (GSs) are oxidized in hot NM liquid to increase their functionalities and subsequently show self-enhanced CAs during the decay. The CAs result from the interatomic exchanges between the functional groups on the sheets and the NM liquid, i.e., mainly between H and O atoms. CA is dependent on the density of NM, functionalities of sheets, and temperature. The GSs and FGSs that originally exhibit different functionalities tend to possess similar functionalities and consequently similar CAs as temperature increases. Other carbon materials and their oxides can accelerate combustion of other fuels/propellants similar to NM, provided that they can be dispersed and their key reaction steps in combustion are similar to NM.

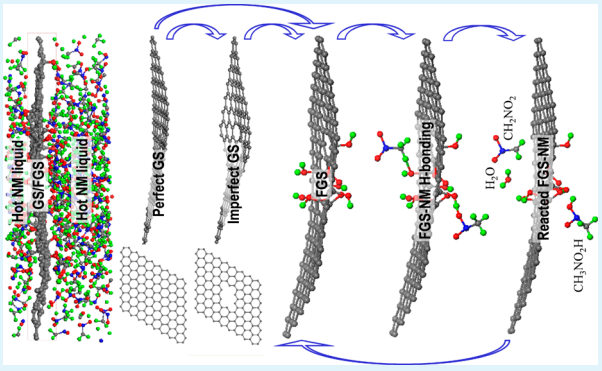

KEYWORDS: *functionalized graphene, self-enhanced catalytic activity, nitromethane, combustion, ReaxFF, molecular dynamics simulations*

INTRODUCTION

Graphene oxide (GO) or the functionalized graphene sheet (FGS)[1] is a promising additive that can accelerate the combustion of nitromethane (NM, CH_3NO_2), a liquid monopropellant. This additive makes the combustion more environmental friendly and strengthens the propulsion with shortened ignition time. FGS can enhance the burning rate of NM by over 175%, showing a much higher catalytic activity (CA) than conventional aluminum monohydroxide and silica nanoparticles in hot NM liquid.[2] The mechanism of NM combustion may be similar to those of propellants that also contain C, H, N and O atoms. Accordingly, FGS application to enhance combustion of fuels/propellants similar to NM is advantageous to the environment.

The determination of the structural changes in the C sheet and the CA of FGS in combustion has attracted much interest. Molecular dynamic (MD) simulations have provided feasible and efficient methods to verify the related complex combustion reactions in the atomic level. To date, numerous complex reactions of shocked or heated explosives,[6−15] combustion,[16−19] and catalyzes[20] have been explored through MD simulations in combination with ab initio (AI) methods,[3] semiempirical methods (e.g., self-consistent charge density-functional tight binding),[4] or molecular reactive force field methods [e.g., reactive force field (ReaxFF)].[5] In particular, ReaxFF MD simulations have become increasingly popular because they can be applied on large-scale systems. In simulation systems with several hundred millions of atoms, the ReaxFF MD method can offer results comparable to AIMD simulations or experiments. In this study, ReaxFF MD simulations were used to study the CA of FGS in the complex thermal decay of liquid NM with various densities and at different temperatures. The simulations illustrated the H and O exchanges between the oxygenated functional groups and NM and its derivatives, which have been recently reported by AIMD simulation.[21] The simulations also elucidated the CA that was observed experimentally.[2] In this study, we have demonstrated that FGSs and pristine graphene sheets (GSs), immersed in hot NM liquid are active and can trap atoms and groups from the liquid to increase their functionalities. Various types of combinations and dissociations, in addition to the aforementioned exchanges on or within the basal sheets, that result in

Received: March 24, 2014
Accepted: July 23, 2014
Published: July 23, 2014

CA relies on the density of NM, the functionality of sheet, and temperature. Specifically, at a low temperature of 2000 or 2400 K, the FGS with higher functionality immersed in a denser NM liquid will cause higher CA. By contrast, the CA does not depend on the original functionality when temperature increases to 3000 K. Self-enhanced CAs of GS or FGSs in thermally decomposing NM has been observed, that is, the sheets become more catalytically active than their primary states after being immersed into hot NM. Presumably, other C materials, such as activated char, C tube, fullerene, and their oxides, can also be oxidized to increase functionalities in the hot NM liquid. These observations provide deep insight into the complex combustion mechanisms and demonstrate the validity of ReaxFF method in related fields.

METHODOLOGIES

Modeling combustion requires adequate structures and conditions. For the structures, C sheets with various functionalities and NM molecules immersing the sheets were considered. For the C sheets, an original cell containing a sheet of 288 C atoms with a periodic boundary condition was obtained by enlarging a unit cell of graphite under a common condition with 12 × 12 × 1 times along its *a*, *b*, and *c* axes, respectively, to a supercell with two C sheets, and then removing one of the sheets. Moreover, the functionalities, namely, the C-to-O (C:O) atomic ratio, were ascertained experimentally. The FGSs have been include diverse oxygenated functional groups, from hydroxyl and epoxide species on the perfect regions of the basal C planes to carbonyl, carboxyl, and lactol groups, at the defects, holes, and edges of the oxidized C sheets.[22] In this study, a divacancy (absence of two C atoms) decorated by two ethers with four additional hydroxyls attached to the C atoms nearby was considered as a functionalized site. Three types of FGSs with nominal C:O ratios of 48, 24, and 12, denoted by FGS_{48}, FGS_{24}, and FGS_{12}, respectively, were obtained by tuning the amounts of functionalized sites on the sheet. Additionally, GS was considered because it represented an extreme case of absence of functionalized site on the sheet. These sheets are illustrated at the bottom of Figure 1b−1e. The consistency of the NM liquid density

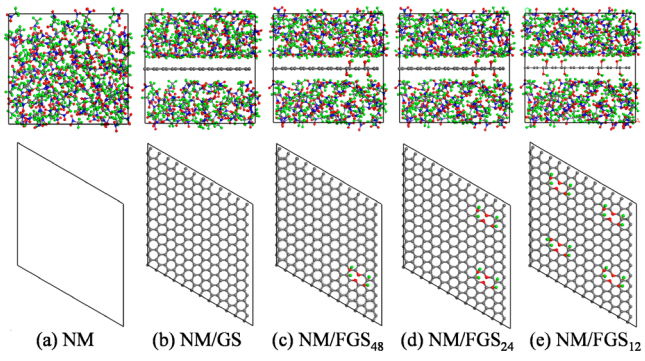

Figure 1. Simulation models for the thermal decomposition of NM on GS and FGSs: (a) pure NM, (b) NM/GS, (c) NM/FGS_{48}, (d) NM/FGS_{24}, and (e) NM/FGS_{12}. The C, H, N, and O atoms are represented in black, green, blue, and red, respectively. Similar representations are considered in the following figures. The top and bottom panels are the side and top views of the basal sheets, respectively.

was maintained because NM decay has been found to be dependent on density.[23] This behavior was confirmed by the simulations in the current study. During construction, C, H, and O atoms were assigned van der Waals radii of 1.70, 1.09, and 1.52 Å, respectively, to evaluate the volumes of the GS and FGSs. Then, the *c*-axial length of the original cell was varied in terms of the evaluated volumes and the NM liquid densities, while the other parameters were kept constant. Meanwhile, a cell with neat 200 NM molecules was constructed, and its decay was used as reference to exhibit CA. The structures, parameters, and components of all modeling cells are shown in Figure 1 and Tables S1 and S2 of Supporting Information, respectively. The top plots in Figure 1b−1e show the GS or FGSs immersed in the NM liquid. Five simulation systems were denoted as NM, NM/GS, NM/FGS_{48}, NM/FGS_{24}, and NM/FGS_{12}. A similar NM/FGS_{22} system was also adopted in the AIMD simulation.[21] The size effect on the simulation results was also considered. Therefore, supplementary simulations on the enlarged cells of NM/FGS_{12} were performed, the effect of size was not verified because no difference in NM decay was observed in Figure S2 of Supporting Information, which suggested the adequateness of employed cell sizes.

Two densities of NM liquid and three temperatures were chosen to simulate combustion conditions. The two densities were d = 1.14 and 1.9 g/cm^3, according to the liquid NM at standard temperature and pressure and the Chapman-Jouget detonation state (steady detonation), respectively. Temperature from frame to bulk liquid sharply decreased during practical NM combustion. The combustion occurred in the region of flame, which was referred to in the simulation. A temperature of 2400 K was assigned as a moderate simulation temperature because this temperature was evaluated to be appropriate for the middle flame.[1] Moreover, high and low temperatures of 3000 and 2000 K, respectively, were also considered. In practice, combustion takes place under moderate conditions among assigned densities and temperatures.

Canonical particle number (N), volume (V), and temperature (T) conditions (NVT) were adopted with the aforementioned densities, temperatures, and functionalities. An improved ReaxFF-lg[24] MD method in LAMMPS package was also employed[25,26] to simulate the related evolution resembling something in the region of the flame where combustion takes place. A total of 30 simulations were performed. Figure 1 shows the five kinds of cells, with each cell covering two densities and three temperatures. The simple Nosé−Hoover thermostat method[27] was employed in these simulations, and the time step and the effective relaxation time were assigned to 0.1 and 20 fs, respectively. Specifically, the coupling frequency of the thermostat to the nuclear motion was composed of 200 time steps. Each cell was relaxed using an NVT MD simulation at 300 K for 10 ps, and no NM decay was found prior to heating to assigned temperatures. Then, 30 independent simulations were performed for 100 ps. Furthermore, supplementary microcanonical (NVE) simulations were performed to resemble an adiabatic extreme in the NM combustion instead of the aforementioned cases under constant temperature. Consequently, both NVE and NVT simulations exhibited self-enhanced CAs of FGSs in the NM decay, as illustrated in Figure S3 of Supporting Information. The result also verified the currently used coupling parameters of the simple Nosé−Hoover thermostat such as those in the study of Page et al.[28] Only NVT simulation results will be discussed later.

The principle of the ReaxFF method can be found in the literature.[5] Briefly, ReaxFF is an improved force field derived from earlier reactive empirical force fields such as those by Brenner,[29,30] parametrized to reproduce the density functional theory (DFT) results for selected systems and properties. It is a molecular force field based on the DFT, in which the formation of a chemical bond is determined by its bond order. ReaxFF has been successfully applied to study the reactions of shocked or heated condensed systems included in energetic materials and fuels.[6−15,15−18] Improved ReaxFF-lg accounts for the dispersion force and can usually provide more accurate predictions than the unenhanced one.[24] In addition, the successful application of improved ReaxFF-lg to the thermal reduction of FGSs[31] and the thermal decomposition of NM[23,24] suggest its validity in the present study, so no revalidation is required.

RESULTS AND DISCUSSION

Thermal NM decay has been considered in various experimental and computational studies[23,32−50] because NM is an ideal prototype of the CHON-based explosives and a

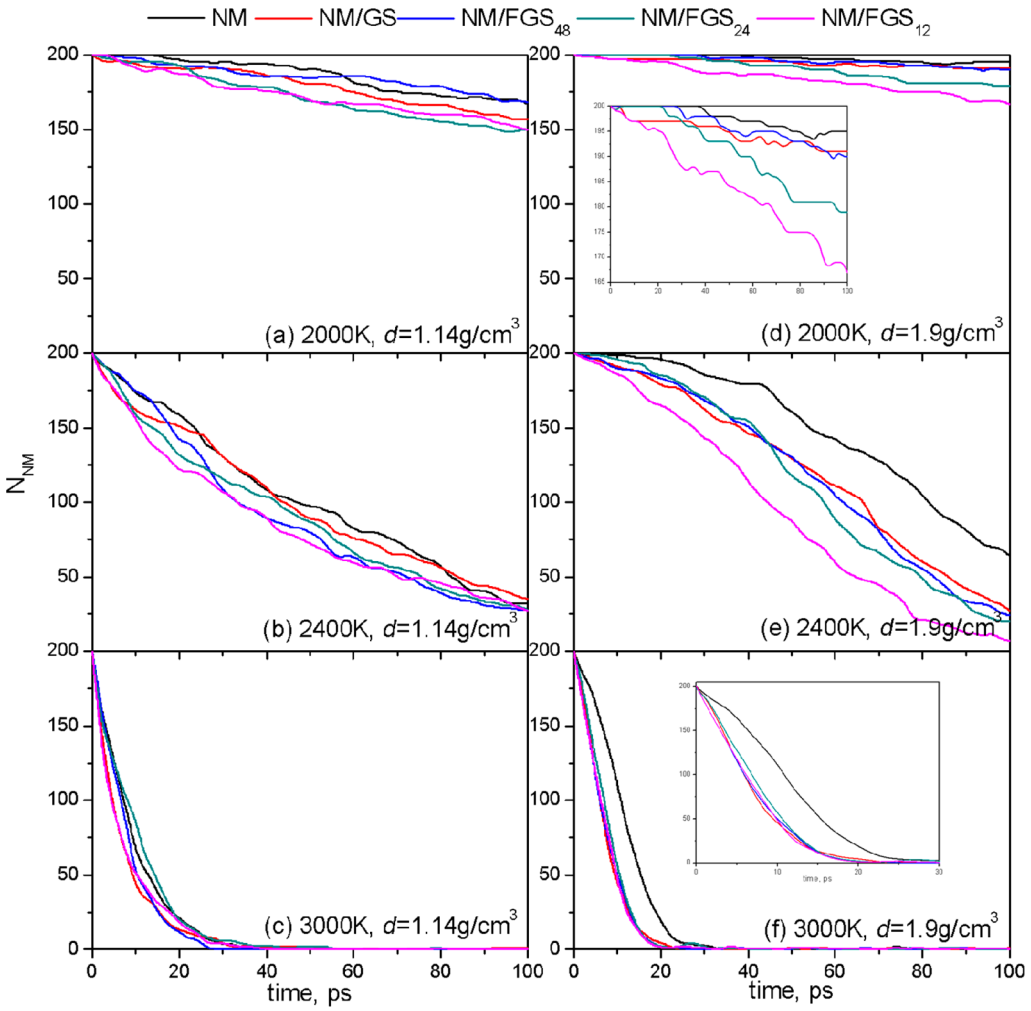

Figure 2. Decay evolution of the hot NM (d = 1.14 g/cm^3) and temperatures of (a) 2000, (b) 2400, and (c) 3000 K; density of 1.9 g/cm^3 and temperatures of (a) 2000, (b) 2400, and (c) 3000 K.

monopropellant in practice. Its thermal decomposition mechanism has been extensively investigated in the field of energetic materials. Additionally, NM decay is initiated primarily by breakage of C−NO_2 and H transfer, which can be distinguished by the different initial intermediates. These initiations are strongly dependent on density, temperature, shock velocity, acid−base degree, and so on. The current study focused on the active site and CA changes in the GS and the FGSs after immersion into the hot NM liquid because the detailed mechanisms have been described previously.[23,32−50]

The decay evolution under various densities and temperatures is illustrated in Figure 2. The CAs of the sheets can be confirmed by comparing the decay rates of NM/GS and NM/FGSs with those of the neat NM liquid. Figure 2 shows that all sheets exhibit CAs conditionally. First, the CA relies on liquid density. No obvious CAs of either the GS or the FGSs are found when accelerating the thermal decomposition with a lower density of NM liquid (d = 1.14 g/cm^3) at 2000, 2400, or 3000 K, without decay distinction in Figure 2a, 2b, or 2c. However, remarkable CAs were observed when the density increases to 1.9 g/cm^3 at the three simulation temperatures, with the decay enhanced in Figure 2d−2f. Surprisingly, the GS, without a primitive active site, also exhibits CA.

The density-dependent CA is strongly related to the reaction mechanisms and active sites on the sheets. Moreover, the initiation mechanism is deduced by the detailed evolution of the initial chemical species (Figure 3 and Figures S4 and S5 of Supporting Information). For the active sites on sheets, the structural variations and their influences on CA, i.e., the intrinsic interatomic exchanges on sheets, are of interest. Typically, the evolution of neat NM liquid, NM/GS (without a primitive active site), and NM/FGS_{12} (with the most primitive active sites) should be clarified. At moderate temperature of 2400 K, at which NO_2 and CH_3NO appear in each plot of Figure 3 with different populations in terms of the densities. NO_2 and CH_3NO corresponds to the decay initiations from C−NO_2 break and H transfer, respectively,[23] The main initial intermediate of NO_2 in Figure 3a−3c corresponds to a lower density of 1.14 g/cm^3. By contrast, Figure 3d−3f represents a higher density of 1.9 g/cm^3 and show the largest populations of CH_3NO. This result implies the density-dependent initial steps. That is, the unimolecular C−NO_2 breakage initiates the decay dominantly at lower density with main intermediates of NO_2, NO, and CH_4, whereas at higher density, the intermolecular reactions govern the decay initiation with the appearance of main species like CH_3NO and OH formed by the equation $2CH_3NO_2 \rightarrow CH_3NO + OH + CH_2NO_2$.[23] Similar results are also derived from the MD simulations at 2000 and 3000 K, as illustrated in Figures S4 and S5 of Supporting Information,

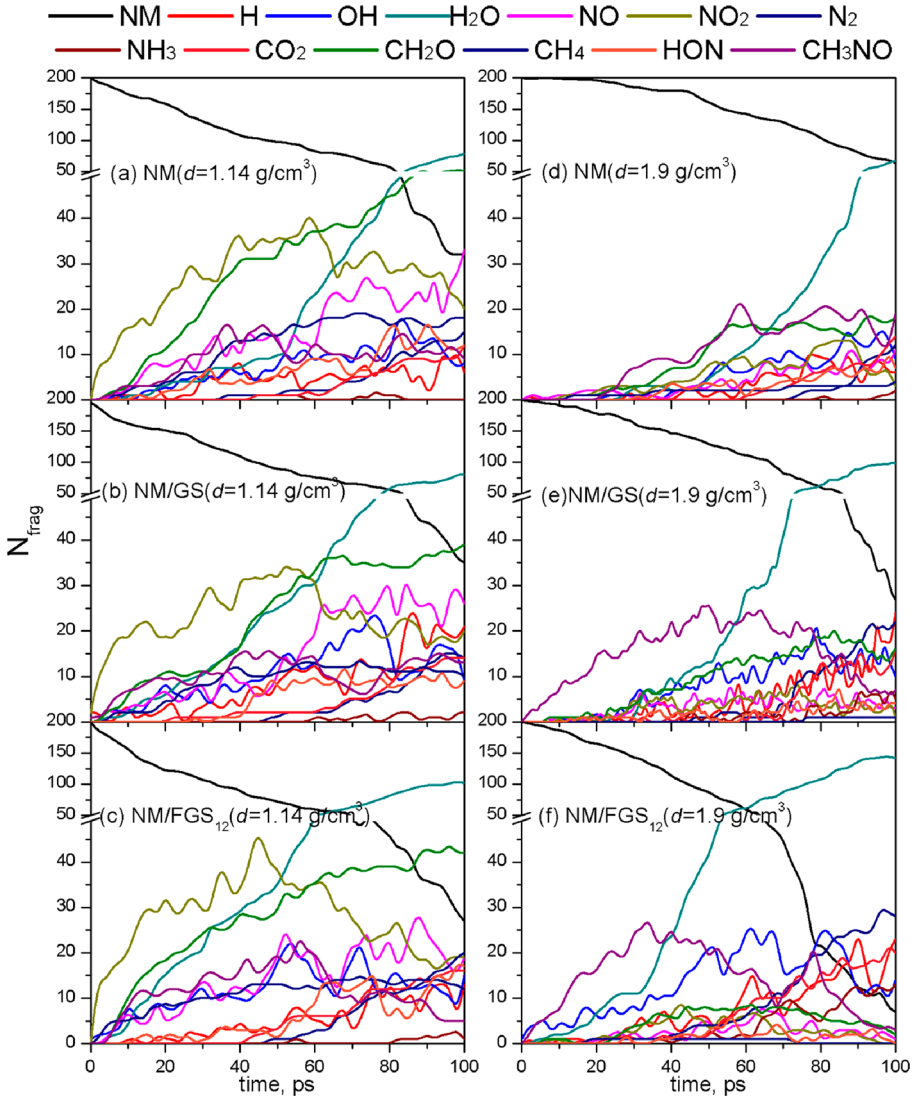

Figure 3. Evolution of main chemical species in the early decay of hot NM at 2400 K. (a) NM, (b) NM/GS, and (c) NM/FGS_{12} at NM density of 1.14 g/cm^3 and (d) NM, (e) NM/GS, and (f) NM/FGS_{12} at NM density of 1.9 g/cm^3 respectively.

respectively. This result agrees with a recent ReaxFF MD simulation on thermal NM decomposition.[24]

This density-dependent initiation mechanism can be elucidated as follows. The bigger free space in a hot NM liquid with a lower density is favorable to stretch C−NO_2 bond as much as possible for breakage. The cleavage of the C−NO_2 bonds predominate the initial decomposition because NO_2 is the dominant intermediate in the initial reactions. By contrast, a compressed free space makes the intermolecular distances shorter, and intermolecular atomic exchanges become easier when the liquid is compressed at a higher density. At this stage, the main intermediate is CH_3NO, which is produced initially by intermolecular H transfers, instead of NO_2 from the C−NO_2 bond break. In addition, we made comparison of plot a with plots b and c and plot d with plots e and f in Figure 3 or those in Figures S4 and S5 of Supporting Information, which show the reactions under a same density−temperature condition. Interestingly, the comparison shows the absence of obvious change in the evolution tendency in the main chemical species when the GS or the FGSs were added into the liquid. This observation suggests that the CAs could mainly be attributed to their roles in accelerating interatomic exchanges, rather than leading to new reactions to form new species. The density-dependent CA needs a prerequisite of intermolecular reactions in the starting decomposition, indicating the catalytic selectivity of the GS and the FGSs in the hot NM liquid. Only cases with 1.9 g/cm^3 density is considered further because CA is exhibited remarkably with higher density.

Temperature is found to evidently affect CA. At 2000 and 2400 K, Figures 2d and 2e show similar increasing decay order of NM, NM/GS, NM/FGS_{48}, NM/FGS_{24}, and NM/FGS_{12}, suggesting that more original functionalized sites may lead to higher CA. The four GS, FGS_{48}, FGS_{24}, and FGS_{12} sheets exhibit comparable CA at 3000 K, regardless of the amount of the original active sites, because the four related decay curves in Figure 2f are almost overlaid. The difference in CAs of the four sheets at 2000 or 2400 K are probably caused by their structural differences, whereas their CA similarity at 3000 K may be because of their structural similarity, at least in the equivalent structures for interatomic transfers in the NM decay. In addition, the CA of the GS suggests a necessary structural change after immersion.

To determine the effect of temperature on the CAs, the structural evolution at different temperatures was examined.

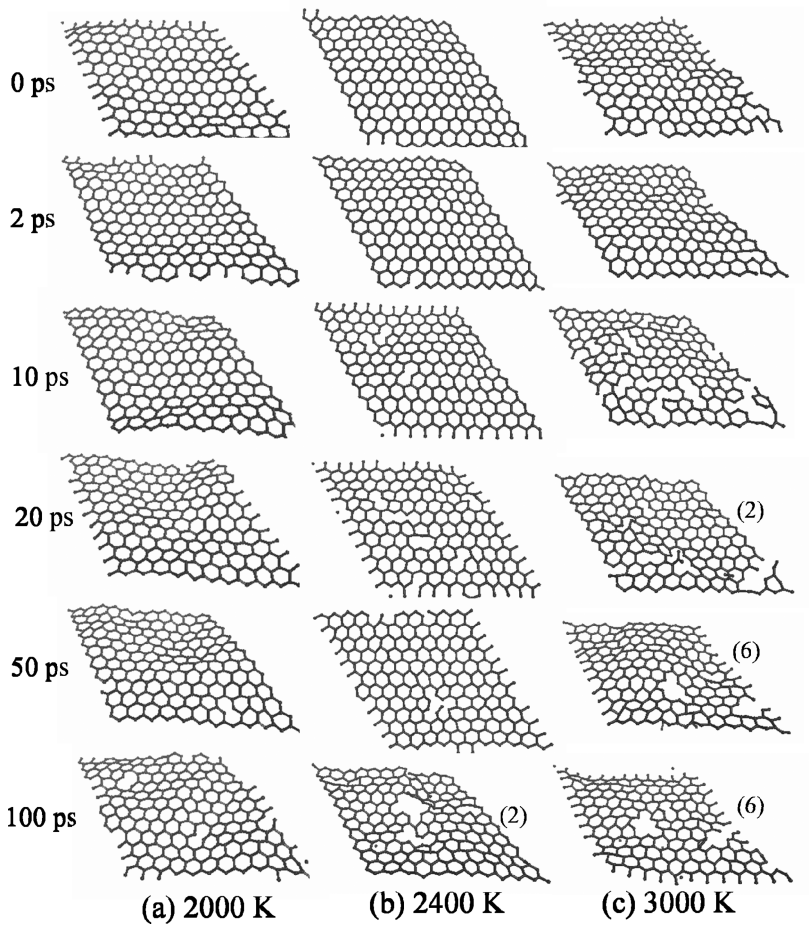

Figure 4. Snapshots of the GS immersed in hot NM liquid (d = 1.9 g/cm^3) under different temperatures of (a) 2000, (b) 2400, and (c) 3000 K. Only primitive C atoms that composed the GS are shown. The number in brackets is the amount of C atoms partitioned completely from the sheet.

Briefly, two typical sheets, GS and FGS_{12}, were employed for discussion. The sheet structures of the immersed GS, along with several representative snapshots, are shown in Figure 4. The sheet is kept almost perfect at 2000 K during simulation, with only few broken C−C bonds although no atom has been completely partitioned away from the basal sheet. Some defects appear on the sheet against 3000 K, but the sheet structure is retained [Figure 4c]. Figure 4c exhibits some vacancies on the sheet, and even some C atoms move far away from the sheet. The result at 2400 K is between those of 2000 and 3000 K [Figure 4b]. In summary, the integrity of the GS is damaged in the hot NM liquid, but its sheet structure is maintained.

The damage may have been caused by high temperatures. To verify this inference, a complementary NVT simulation on an isolated GS against a much higher temperature of 4000 K was performed. Results show that the GS is still perfect, despite the induction of a waved sheet (Figure S6 in Supporting Information). Thus, the defects on the immersed GS result from the NM liquid with heat treatment. The high temperature leads to a waved C sheet and dangling sp^2 C atoms. An isolated GS in Figure S6 of Supporting Information shows that no atom or group is active enough to provide electrons to saturate these transient dangling sp^2 C atoms at 4000 K, leading to a quick return to stable sheet and thus a perfect sheet is produced all along. On the contrary, for the GS immersed in the hot NM liquid, the sp^2 bonds can be saturated by trapping the active NM molecules and their derivatives. The formation of stable sp^3 bonds damages the original planarity of the C sheet and lowers its stability. Subsequently, some C atoms that are originally within the sheet become active and dissociated from the sheet, thereby leading to defects. Subsequently, some NM derivatives in the liquid bond covalently to the regions of the perfect sheet and the defects. Figure 5 exhibits these combinations on the perfect plane and decorations of the defects, as expected. Comparative results from Figure 5a−5c show an increasing amount of atoms and groups that are quickly chemically bonded to the GS as temperature increases. The atoms that are bonded directly to the sheet include all four kinds of atoms. The O atoms occupy the most population to form cyclic ether, carbonyl, hydroxyl, or oxatyl groups. H and N atoms also saturate the dangling sp^2 C atoms within the sheet, and some bigger fragments are chemically linked with the sheet through O, C, or N atoms. The oxidation of the GS to GO or FGS in the hot NM liquid and its CA enhancement is then inferred to be self-induced. In other words, the enhanced CA is derived from the damage and decoration caused by the hot NM liquid. These results are in agreement with recent DFT calculations,[51−54] suggesting the efficiency of ReaxFF to accurately describe carbonaceous systems.

A similar case was observed with FGS_{12}. Some atoms, particularly O and H atoms, become transferable to partition from the sheet as time proceeds, and this process becomes faster as temperature increases (Figure 6). In Figure 6b and 6c, some primitive C atoms within the sheet leave the sheets into

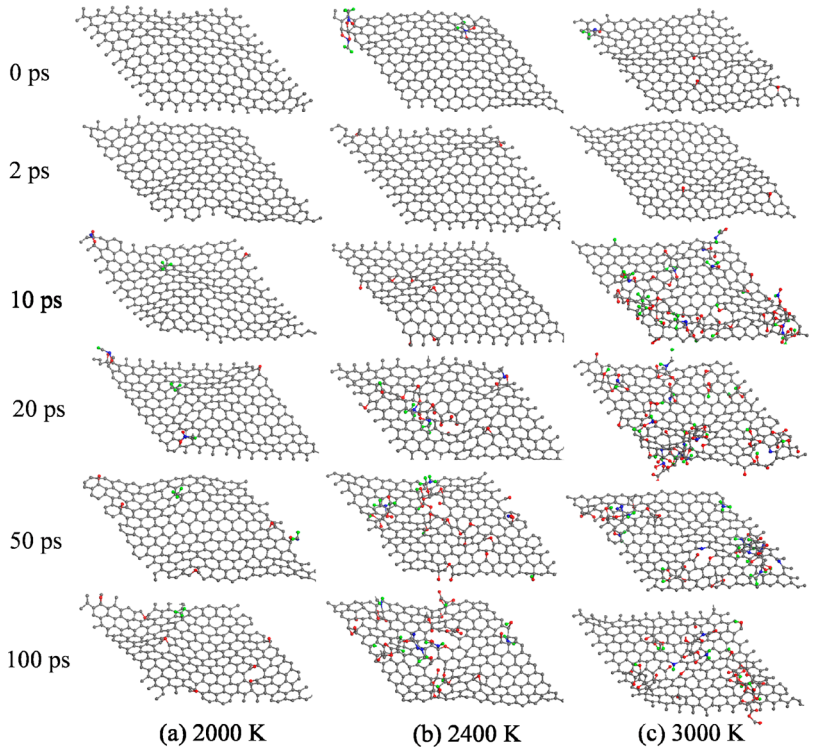

Figure 5. Snapshots of the GS immersed in the hot NM liquid (d = 1.9 g/cm^3) under different temperatures of (a) 2000, (b) 2400, and (c) 3000 K. All atoms bound chemically to the GS are shown.

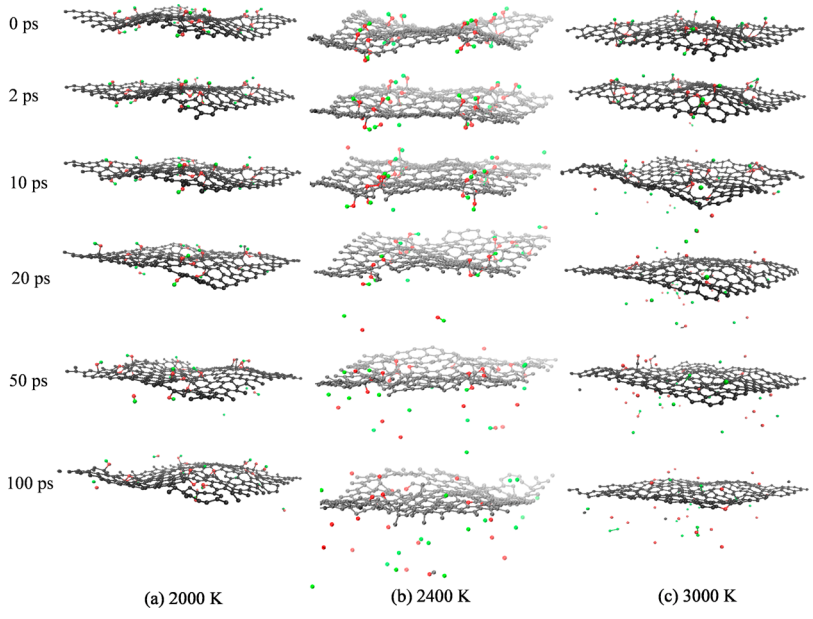

Figure 6. Snapshots of FGS_{12} immersed in the hot NM liquid (d = 1.9 g/cm^3) under different temperatures (a) 2000, (b) 2400, and (c) 3000 K. Only primitive atoms belonging to FGS_{12} are shown.

the hot liquid, suggesting the formation of new defects. To verify this observation, the sheet structures of the GS and FGS_{12} immersed for 100 ps at 2400 K were compared by removing all atoms out of the sheets. Two sheets were obtained and are shown in Figure S7 of Supporting Information. The result shows that the functionalized defects on the GS increase from zero to two, and those on FGS_{12} increase from four to five, suggesting the varied sheet structure and functionality of either the GS or FGS_{12} when immersed in hot NM liquid. Immersion leads to improved chemical adsorption of active NM derivatives on the sheets, indicating the enhanced functionalities or CAs. Moreover, various modes for saturating the defects on the sheets, in addition to O atoms, have also been found (Figure S7 of Supporting Information). Comparative results from the defect sites on sheets in Figure 1e and Supporting Information Figure S7(b) show that the defects are not yet fixed after immersion, suggesting the saturation by C atoms and another mechanism to reduce FGS. Figure 7 shows

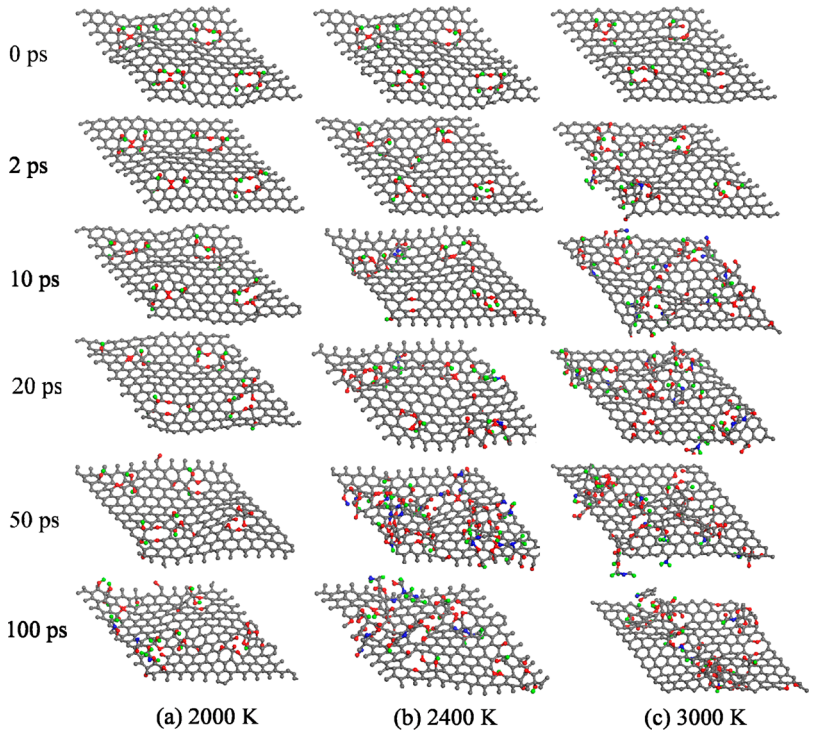

Figure 7. Snapshots of FGS_{12} immersed in the hot NM liquid (d = 1.9 g/cm^3) under different temperatures (a) 2000, (b) 2400, and (c) 3000 K. All atoms bonded chemically with FGS_{12} are shown.

the decorated FGS_{12} in the hot NM liquid as time proceeds. Contrary to Figure 6, which shows the partition of the primitive atoms away from the sheets, the interatomic exchanges on the sheets can be established in Figure 7. That is, the initial atoms on the sheets leave the sheets, and those in the liquid eventually decorate the sheets. FGSs are not consumed in the hot NM liquid at this stage, probably because of the oxidizer-deficiency of NM. Another complementary simulation of NM/FGS_{12} at 3500 K for 200 ps did not show consumption of the sheet (Figure S8 in Supporting Information). Thus, FGS_{12} is also oxidized in the hot NM liquid through interatomic exchanges between the sheet and the liquid.

Hence, both GS and FGS_{12} are oxidized to increase functionalities by immersion in hot NM liquid, while the sheets are maintained all along. The oxidation can be also confirmed by examining the amounts (Δn) of atoms chemically bonded to the basal sheets and the summed molecular weights (MWs) of the sheets and the fragments absorbed chemically on the sheets as the simulations proceed. In the GS, as illustrated in Figure 8a−8c, the four kinds of atoms are linked with the sheet increase. At 2000 and 2400 K, O atoms show the highest increase, followed by the H atoms, while C and N atoms exhibit the lowest increase. At 3000 K, C atoms increase lesser than the O atoms but more than the H atoms after 20 ps, suggesting some bigger fragments, besides O and H atoms, are adsorbed on the sheet, which are detected in the snapshots shown in Figure 5c. At all times, the increased N atoms are limited within a small range. In FGS_{12}, the main difference relative to the GS is the occasional decrease in H atoms [Figure 8d−8f], suggesting the interatomic exchanges between the sheet and the hot NM liquid, consistent with above discussions. From Figure 8g−8i, the MW of the GS is larger than that of FGS_{12} at 2000 and 2400 K; whereas at 3000 K, both MW curves fluctuate in a similar range. This observation implies that GS and FGS_{12} oxidized in the NM liquid at 3000 K possess similar statistic structures, whether functionalized in advance or not. The difference in the atomic amounts between Figure 8c and 8f could be counteracted because the original component difference of GS and FGS_{12}, C_{288} versus $C_{280}O_{24}H_{16}$, had been considered. The primarily less C atoms, as well as the more O and H atoms of FGS_{12}, are counteracted by the more increased C atoms, the less increased O atom, and the decreased H atoms, leading to its statistic structure similar to GS.

Accordingly, temperature dependence of CAs is determined by the amounts of functionalized sites on the four sheets. Fundamentally, at a low temperature of 2000 or 2400 K, the oxidation of the hot NM liquid is limited, therefore the CAs of the GS and the FGSs can be differentiated through their primary structures. However, at a high temperature of 3000 K, four sheets possess similar amounts of functionalized sites or similar abilities to exchange atoms, leading to similar CAs. For example, partitioning the decorated sheets in Figures 5c and 7c is difficult at 100 ps.

The CAs in the NM decay are inferred to be involved in accelerating the atomic exchanges. O and H atoms linked originally with the C sheets are partitioned from the sheet as time proceeds (Figure 6). Even the C atoms are partitioned at high temperatures of 2400 and 3000 K during simulation. Higher temperature causes quicker partition. To resaturate the sites where partition occurs, several active NM molecules or NM derivatives in the hot liquid combine chemically with the liquid. Many atoms or groups decorate the sheets in Figure 7, instead of remaining unsaturated like the hanging bonds after the partition. This result suggests the atomic exchanges between the C sheets and the NM liquid. In most cases, the exchanges are of the O and H atoms, as reported in the AIMD simulation.[21] The detected exchanges of C and N atoms are few

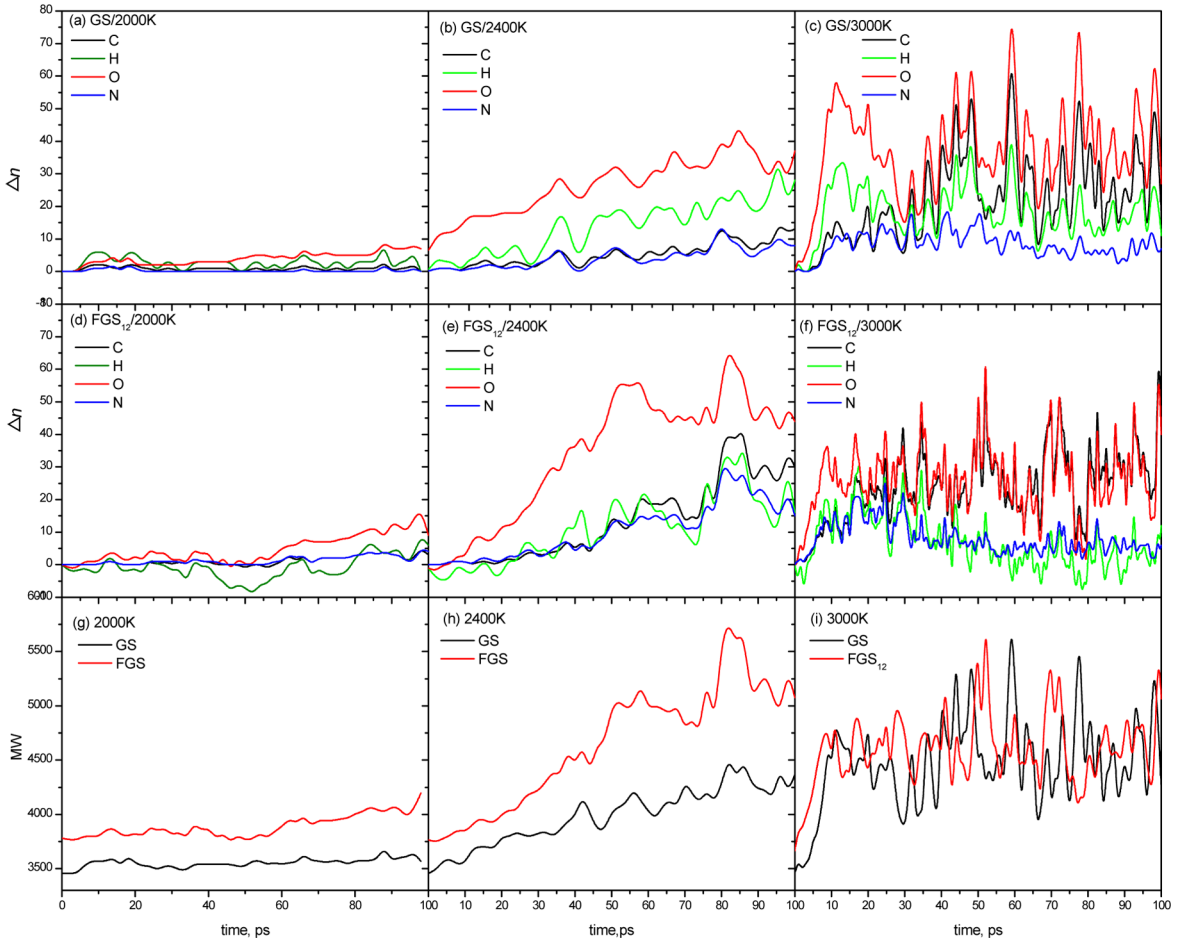

Figure 8. Evolution of changed amounts (Δn) of C, H, O, and N atoms bound to the C sheets: GS at (a) 2000, (b) 2400, and (c) 3000 K, FGS_{12} at (d) 2000, (e) 2400, and (f) 3000 K, and evolution of summed molecular weights (MW) of the sheet with chemically adsorbed fragments at (g) 2000, (h) 2400, and (i) 3000 K.

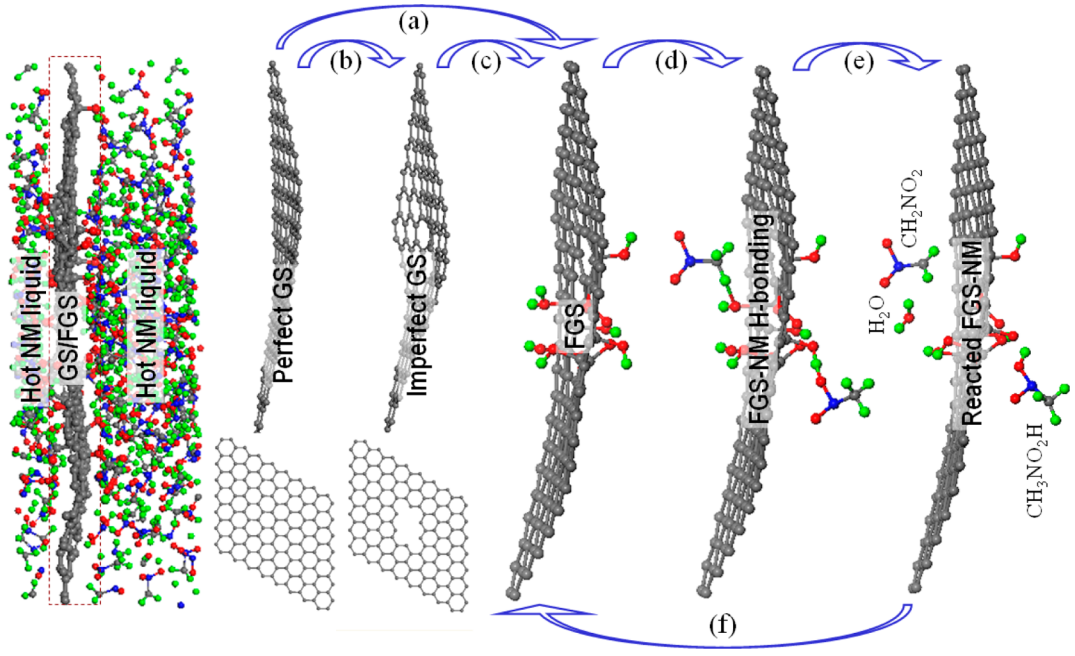

Figure 9. Functionalization of GS and further functionalization of FGSs, and their CAs in hot NM decay: (a) functionalization of GSs, (b) formation of defects, (c) decoration of defects, and (d–f) atomic exchanges between the C sheets and the NM liquid, showing CA.

(Supporting Information Figure S7), but this phenomenon has not been reported.

CONCLUSIONS

In summary, serial ReaxFF MD simulations are used to study the CAs of FGSs in NM combustion. The results show that CAs are dependent on the density of the NM liquid and on the temperature and functionality of the sheet. For example, higher CA is found for more compressed NM liquid, suggesting the catalytic selectivity of FGSs in intermolecular atomic exchanges. At relatively low temperatures of 2000 and 2400 K, CA is dependent on the primary functionalities of the sheets, whereas at 3000 K the functionality dependence of CA disappeared. More importantly, both GS and FGS are oxidized to increase functionality in hot NM liquid, which lead to equivalent structures that accelerate interatomic exchanges or a similar CA at 3000 K. Figure 9 shows a summary of a related process. The CA of GSs or FGSs increases in the hot NM liquid, and some active NM molecules or their derivatives in the liquid are adsorbed chemically on the sheets where the dangling sp^2 bonds appear by heating. The chemical adsorption can also be completed through the initial formation of defects, such as vacancies and hanging bonds on the sheets, and subsequent decoration by the hot NM liquid. FGSs accelerate the NM decay through the atomic exchanges between the C sheets and the NM liquid. Moreover, the adsorptions and the exchanges are repeated until reactions are completed. In addition, the sheet is not consumed during the simulations, which may be attributed to the oxidizer-deficiency of the NM liquid.

Other C materials with similar sp^2 bonds, such as the C tube, fullerene, and activated char,[55] may become dangled and can be oxidized to increase functionality in hot NM liquid and in other propellants/fuels similar to NM. Therefore, the CAs of these C materials and their oxides are proposed in the combustion of various propellants/fuels if they can be dispersed and their combustion processes follow key steps similar to NM.

Therefore, the CA of FGS, which results from the intermolecular atomic exchanges between the sheets and the liquid, is most determined by the functionalities of the sheets. The functionality is crucial to CA. FGS is much more active than GS because of the higher functionality of FGS. The enhanced CAs of the GS and FGSs in hot NM liquid are attributed to their increased functionalities. Moreover, GS and FGSs show similar CAs in NM liquid at 3000 K because of their similar functionalities.

ASSOCIATED CONTENT

Supporting Information

Lattice parameters and components of simulation cells, supplementary simulations for verifying no size effect on results, supplementary NVE simulations, evolution of main chemical species in the early decay of NM at 2000 and 3000 K, evolution of the isolated carbon sheet against 4000 K, sheet structure comparison of the GS and FGS_{12} immersed in hot NM liquid at 2400 K for 100 ps, and snapshots of NM/FGS_{12} against 3500 K as time proceeds 100 and 200 ps. This material is available free of charge via the Internet at http://pubs.acs.org/.

AUTHOR INFORMATION

Corresponding Author

*E-mail: chaoyangzhang@caep.cn.

Notes

The authors declare no competing financial interest.

ACKNOWLEDGMENTS

We are greatly grateful for the financial support from the Science and Technology Fund of CAEP (2011A0302014), the Science and Technology Innovation Fund of ICM (KJCX-201305) and the National Natural Science Foundation of China (21173199).

REFERENCES

(1) Stankovich, S.; Dikin, D. A.; Dommett, G. H. B.; Kohlhaas, K. M.; Zimney, E. J.; Stach, E. A.; Piner, R. D.; Nguyen, S. T.; Ruoff, R. S. Graphene-Based Composite Materials. *Nature* **2006**, *442*, 282−286.

(2) Justin, L.; Daniel, M.; Richard, A.; Frederick, L.; Ilhan, A. Functionalized Graphene Sheet Colloids for Enhanced Fuel/propellant Combustion. *ACS Nano* **2009**, *3*, 3945−3954.

(3) Car, R.; Parrinello, M. Unified Approach for Molecular Dynamics and Density-Functional Theory. *Phys. Rev. Lett.* **1985**, *55*, 2471.

(4) Elstner, M.; Porezag, D.; Jungnickel, G.; Elsner, J.; Hauk, M.; Frauenheim, T.; Suhai, S.; Seifert, G. Self-Consistent-Charge Density-Functional Tight-Binding Method for Simulations of Complex Materials Properties. *Phys. Rev. B* **1998**, *58*, 7260.

(5) Chakraborty, D.; Muller, R. P.; Dasgupta, S.; Goddard, W. A., III. Mechanism for Unimolecular Decomposition of HMX (1,3,5,7-Tetranitro-1,3,5,7-tetrazocine), an Ab Initio Study. *J. Phys.Chem. A* **2001**, *105*, 1302−1314.

(6) Strachan, A.; van Duin, A. C. T.; Chakraborty, D.; Dasgupta, S.; Goddard, W. A., III. Shock Waves in High-Energy Materials: The Initial Chemical Events in Nitramine RDX. *Phys. Rev. Lett.* **2003**, *91*, No. 098301.

(7) Nomura, K. I.; Kalia, R. K.; Nakano, A.; Vashishta, P.; van Duin, A. C. T; Goddard, W. A., III. Dynamic Transition in the Structure of an Energetic Crystal during Chemical Reactions at Shock Front prior to Detonation. *Phys. Rev. Lett.* **2007**, *99*, No. 148303.

(8) Ge, N. N.; Wei, Y. K.; Ji, G. F.; Chen, X. R.; Zhao, F.; Wei, D. Q. Initial Decomposition of the Condensed-phase β-HMX under Shock Waves: Molecular Dynamics Simulations. *J. Phys. Chem. B* **2012**, *116*, 13696−13704.

(9) Manaa, M. R.; Reed, E. J.; Fried, L. E.; Goldman, N. Nitrogen-Rich Heterocycles as Reactivity Retardants in Shocked Insensitive Explosives. *J. Am. Chem. Soc.* **2009**, *131*, 5483−5487.

(10) Reed, E. J.; Manaa, M. R.; Fried, L. E.; Glaesemann, K. R.; Joannopoulos, J. D. A Transient Semimetallic Layer in Detonating Nitromethane. *Nat. Phys.* **2008**, *4*, 72−76.

(11) Zybin, S. V.; Goddard, W. A., III.; Xu, P.; van Duin, A. C. T; Thompson, A. P. Physical Mechanism of Anisotropic Sensitivity in Pentaerythritol Tetranitrate from Compressive-Shear Reaction Dynamics Simulations. *Appl. Phys. Lett.* **2010**, *96*, No. 081918.

(12) Han, S. P.; van Duin, A. C. T; Goddard, W. A., III.; Strachan, A. Thermal Decomposition of Condensed-Phase Nitromethane from Molecular Dynamics from ReaxFF Reactive Dynamics. *J. Phys. Chem. B* **2011**, *115*, 6534−6540.

(13) Zhou, T. T.; Zybin, S. V.; Liu, Y.; Huang, F. L.; Goddard, W. A., III. Anisotropic Shock Sensitivity for β-Octahydro-1,3,5,7-tetranitro-1,3,5,7-tetrazocine Energetic Material under Compressive-shear Loading from ReaxFF-lg Reactive Dynamics Simulations. *J. Appl. Phys.* **2012**, *111*, 124904.

(14) Shan, T.; Wixom, R.; Mattsson, A.; Thompson, A. Atomistic Simulation of Orientation Dependence in Shock-induced Initiation of Pentaerythritol Tetranitrate. *J. Phys. Chem. B* **2013**, *117*, 928−936.

(15) Nomura, K.; Kalia, R. K.; Nakano, A.; Vashishta, P. Reactive Nanojets: Nanostructure Enhanced Chemical Reactions in A Defected Energetic Crystal. *Appl. Phys. Lett.* **2007**, *91*, No. 183109.

(16) Fidel, C. M.; Amar, M. K.; Michael, F. R., Jr.; van Duin, A. C. T.; Jonathan, P. M. Combustion of An Illinois No. 6 Coal Char Simulated Using An Atomistic Char Representation and the ReaxFF Reactive Force Field. *Combust. Flame* **2012**, *159*, 1272−1285.

(17) Wang, Q.; Wang, J.; Li, J.; Tan, N.; Li, X. Reactive Molecular Dynamics Simulation and Chemical Kinetic Modeling of Pyrolysis and Combustion of n-dodecane. *Combust. Flame* **2011**, *158*, 217−226.
(18) Fidel, C. M.; van Duin, A. C. T. Comparison of Thermal and Catalytic Cracking of 1-heptene from ReaxFF Reactive Molecular Dynamics Simulations. *Combust. Flame* **2013**, *160*, 766−775.
(19) Ding, J.; Zhang, L.; Zhang, Y.; Han, K. A Reactive Molecular Dynamics Study of n-heptane Pyrolysis at High Temperature. *J. Phys. Chem. A* **2013**, *117*, 3266−3278.
(20) Raju, M.; Kim, S.; van Duin, A.; Fichthorn, K. ReaxFF Reactive Force Field Study of the Dissociation of Water on Titania Surfaces. *J. Phys. Chem. C* **2013**, *117*, 10558−10572.
(21) Liu, L.; Car, R.; Selloni, A.; Dabbs, D. M.; Aksay, I. A.; Yetter, R. A. Enhanced Thermal Decomposition of Nitromethane on Functionalized Graphene Sheets: Ab initio Molecular Dynamics Simulations. *J. Am. Chem. Soc.* **2012**, *134*, 19011−19016.
(22) Dreyer, D. R.; Park, S.; Bielawski, C. W.; Ruoff, R. S. The Chemistry of Graphene Oxide. *Chem. Soc. Rev.* **2010**, *39*, 228−240 and references therein..
(23) Rom, N.; Zybin, S. V.; van Duin, A. C. T.; Goddard, W. A.; Zeiri, Y.; Katz, G.; Kosloff, R. Density-dependent Liquid Nitromethane Decomposition: Molecular Dynamics Simulations Based on ReaxFF. *J. Phys. Chem. A* **2011**, *115*, 10181−10202.
(24) Liu, L. C.; Liu, Y.; Zybin, S. V.; Sun, H.; Goddard, W. A., III. ReaxFF-lg: Correction of the ReaxFF Reactive Force Field for London Dispersion, with Applications to the Equations of State for Energetic Materials. *J. Phys. Chem. A* **2011**, *115*, 11016−11022.
(25) Plimpton, S. J. Fast Parallel Algorithms for Short-Range Molecular Dynamics. *J. Comput. Phys.* **1995**, *117*, 1−19.
(26) Aktulga, H. M.; Fogarty, J. C.; Pandit, S. A.; Grama, A. Y. Parallel Reactive Molecular Dynamics: Numerical Methods and Algorithmic Techniques. *Parallel Comput.* **2012**, *38*, 245−259.
(27) Hoover, W. Canonical Dynamics: Equilibrium Phase-Space Distributions. *Phys. Rev. A* **1985**, *31*, 1695−1697.
(28) Page, A. J.; Isomoto, T.; Knaup, J. M.; Irle, S.; Morokuma, K. Effects of Molecular Dynamics Thermostats on Descriptions of Chemical Nonequilibrium. *J. Chem. Theory Comput.* **2012**, *8*, 4019−4028.
(29) Brenner, D. W. Empirical Potential for Hydrocarbons for Use in Simulating the Chemical Vapor Deposition of Diamond Films. *Phys. Rev. B* **1990**, *42*, 9458−9471.
(30) Brenner, D. W.; Shenderova, O. A.; Harrison, J.; Stuart, S. J.; Ni, B.; Sinnott, S. B. A Second-Generation Reactive Empirical Bond Order (REBO) Potential Energy Expression for Hydrocarbons. *J. Phys.: Condens. Matter* **2002**, *14*, 783−802.
(31) Bagri, A.; Mattevi, C.; Acik, M.; Chabal, Y. J.; Chhowalla, M.; Shenoy, V. B. Structural Evolution during the Reduction of Chemically Derived Graphene Oxide. *Nat. Chem.* **2010**, *2*, 581−587.
(32) Macaveiu, L.; Göbel, M.; Klapötke, T. M.; Murray, J. S.; Politzer, P. The Unique Role of the Nitro Group in Intramolecular Interactions: Chloronitromethanes. *Struct. Chem.* **2010**, *21*, 139−146.
(33) Bull, J. N.; Maclagan, R. G. A. R.; Harland, P. W. On the Rlectron Sffinity of Nitromethane (CH_3NO_2). *J. Phys. Chem. A* **2010**, *114*, 3622−3629.
(34) Zhu, R. S.; Lin, M. C. CH_3NO_2 Decomposition/Isomerization Mechanism and Product Branching Ratios: An Ab Initio Chemical Kinetic Study. *Chem. Phys. Lett.* **2009**, *478*, 11−16.
(35) Murray, J. S.; Lane, P.; Göbel, M.; Klapötke, T. M.; Politzer, P. Intra- and Intermolecular Electrostatic Interactions and Their Significance for the Structure, Acidity, and Tautomerization Behavior of Trinitromethane. *J. Chem. Phys.* **2009**, *130*, No. 104304.
(36) Guo, Y. Q.; Bhattacharya, A.; Bernstein, E. R. Photodissociation Dynamics of Nitromethane at 226 and 271 nm at Both Nanosecond and Femtosecond Time Scales. *J. Phys. Chem. A* **2009**, *113*, 85−96.
(37) Goebbert, D. J.; Pichugin, K.; Sanov, A. Low-Lying Electronic States of CH_3NO_2 via Photoelectron Imaging of the Nitromethane Anion. *J. Chem. Phys.* **2009**, *131*, No. 164308.
(38) Adams, C. L.; Schneider, H.; Ervin, K. M.; Weber, J. M. Low-Energy Photoelectron Imaging Spectroscopy of Nitromethane Anions: Electron Affinity, Vibrational Features, Anisotropies, and the Dipole-Bound State. *J. Chem. Phys.* **2009**, *130*, 074307.
(39) Wade, E. A.; Reak, K. E.; Li, S. L.; Clegg, S. M.; Zou, P.; Osborn, D. L. Time-Dependent Infrared Emission Following Photodissociation of Nitromethane and Chloropicrin. *J. Phys. Chem. A* **2006**, *110*, 4405−4412.
(40) McKee, M. L. Ab Initio Study of Rearrangements on the Nitromethane Potential Energy Surface. *J. Am. Chem. Soc.* **1986**, *108*, 5784−5792.
(41) Dewar, M. J. S.; Ritchie, J. P.; Alster, J. Thermolysis of Molecules Containing NO_2 Groups. *J. Org. Chem.* **1985**, *50*, 1031−1036.
(42) Manelis, G. B. *Thermal Decomposition and Combustion of Explosives and Propellants*; Taylor & Francis: London, 2003.
(43) Siavosh-Haghighi, A.; Dawes, R.; Sewell, T. D.; Thompson, D. L. Shock-Induced Melting of (100)-Oriented Nitromethane: Structural Relaxation. *J. Chem. Phys.* **2009**, *131*, No. 064503.
(44) Citroni, M.; Datch, F.; Bini, R.; Vaira, M. D.; Pruzan, P.; Canny, B.; Schettino, V. Crystal Structure of Nitromethane up to the Reaction Threshold Pressure. *J. Phys. Chem.B* **2008**, *112*, 1095−1103.
(45) Zerilli, F. J.; Hooper, J. P.; Kuklja, M. M. Ab Initio Studies of Crystalline Nitromethane under High Pressure. *J. Chem. Phys.* **2007**, *126*, No. 114701.
(46) Megyes, T.; Bálint, S.; Grósz, T.; Radnai, T.; Bakó, I.; Almásy, L. Structure of Liquid Nitromethane: Comparison of Simulation and Diffraction Studies. *J. Chem. Phys.* **2007**, *126*, 164507.
(47) Siavosh-Haghighi, A.; Thompson, D. L. Molecular Dynamics Simulations of Surface-Initiated Melting of Nitromethane. *J. Chem. Phys.* **2006**, *125*, No. 184711.
(48) Liu, H.; Zhao, J.; Wei, D.; Gong, Z. Structural and Vibrational Properties of Solid Nitromethane under High Pressure by Density Functional Theory. *J. Chem. Phys.* **2006**, *124*, No. 124501.
(49) Alavi, S.; Thompson, D. L. A Molecular-Dynamics Study of Structural and Physical Properties of Nitromethane Nanoparticles. *J. Chem. Phys.* **2004**, *120*, No. 10231.
(50) Engelke, R.; Sheffield, S. A.; Stacy, H. L. Effect of Deuteration on the Diameter−Effect Curve of Liquid Nitromethane. *J. Phys. Chem. A* **2006**, *110*, 7744−7748.
(51) Garcia-Fernandez, C.; Picaud, S.; Rayez, M. T.; Rayez, J. C.; Rubayo-Soneira, J. First-Principles Study of the Interaction between NO and Large Carbonaceous Clusters Modeling the Soot Surface. *J. Phys. Chem. A* **2014**, *118*, 1443−1450.
(52) Oubal, M.; Picaud, S.; Rayez, M.; Rayez, J. Water Adsorption on Oxidized Single Atomic Vacancies Present at the Surface of Small Carbonaceous Nanoparticles Modeling Soot. *ChemPhysChem* **2010**, *11*, 4088−4096.
(53) Oubal, M.; Picaud, S.; Rayez, M.; Rayez, J. Adsorption of Atmospheric Oxidants at Divacancy Sites of Graphene: A DFT Study. *Comput. Theor. Chem.* **2013**, *1016*, 22−27.
(54) Oubal, M.; Picaud, S.; Rayez, M.; Rayez, J. Structure and Reactivity of Carbon Multivacancies in Graphene. *Comput. Theor. Chem.* **2012**, *990*, 159−166.
(55) Zhang, J.; Liu, X.; Blume, R.; Zhang, A.; Schlögl, R.; Su, D. S. Surface-Modified Carbon Nanotubes Catalyze Oxidative Dehydrogenation of *n*-Butane. *Science* **2008**, *322*, 73−77.